

Fission of polonium, osmium, and erbium composite systems

J. van der Plicht,* H. C. Britt, M. M. Fowler, Z. Fraenkel,† A. Gavron, and J. B. Wilhelmy
Los Alamos National Laboratory, Los Alamos, New Mexico 87545

F. Plasil, T. C. Awes, and G. R. Young
Oak Ridge National Laboratory, Oak Ridge, Tennessee 37830
 (Received 5 July 1983)

Fission cross section excitation functions were measured from near threshold to ~ 10 MeV/nucleon using ^9Be , ^{12}C , $^{16,18}\text{O}$, $^{24,26}\text{Mg}$, ^{32}S , and ^{64}Ni beams. The systems studied included ^{210}Po formed in ^{12}C and ^{18}O induced reactions; ^{186}Os formed in ^9Be , ^{12}C , ^{16}O , and ^{26}Mg reactions; and ^{158}Er formed in ^{16}O , ^{24}Mg , ^{32}S , and ^{64}Ni reactions. In addition, the composite systems $^{204,206,208}\text{Po}$ formed with ^{16}O and ^{18}O projectiles were studied. In the experiment the velocities and emission angles of two coincident fission fragments were measured using position-sensitive multiwire proportional counter stop detectors and a thin ($\sim 200 \mu\text{g}/\text{cm}^2$) gas "start" detector. The measured fission excitation functions along with previous data from ^4He and ^{11}B bombardments for the ^{186}Os and ^{210}Po systems and recent data on the ^{200}Pb system are compared to statistical model calculations using recent angular momentum dependent fission barriers calculated by Sierk. Comparisons of calculated and measured fission excitation functions show good overall agreement between data and theoretical predictions. These comparisons give good agreement for both a wide range of mass of the composite system and for a wide range of mass asymmetry in the entrance channel. It is concluded that the fission barriers of Sierk give a good description of both the mass and angular momentum dependence of fission barriers in this region.

I. INTRODUCTION

There have been many studies¹ of fission probabilities in the actinides that have yielded a comprehensive mapping of fission-barrier parameters in this region. In order to understand these results quantitatively, it was necessary to include effects of nuclear shells and fundamental shape symmetries at the saddle point. For lighter nuclei, fission barriers ($l=0$) become large compared to neutron binding energies, but for large angular momenta fission can again become a dominant process due to the centrifugal lowering of the barrier. In this region, the limited experimental results have been fit with various statistical model codes²⁻¹⁰ primarily utilizing calculated fission barriers from the rotating liquid drop model (RLDM) of Cohen, Plasil, and Swiatecki¹¹ (CPS). In fits to fission cross sections it has generally been necessary to lower the CPS barriers using an arbitrary renormalization procedure. Because of the limited data available and the need to renormalize, it has not yet been possible to systematically test the predicted angular momentum dependence of the fission barrier. However, a more recent angular-momentum-dependent barrier calculation by Sierk¹² has been shown⁹ to give a good representation of data to the composite systems ^{153}Tb and ^{181}Re without the necessity for renormalizing the calculated barrier heights. Because of the limited data and uncertainties in the RLDM-barrier calculations, it has not been possible to obtain any significant estimates of the importance of shell effects on fission barriers in the mass ≤ 210 region.

The purpose of the present experiment was to develop a representative set of fission cross-section data, so that it

would be possible to test both the mass and angular momentum dependence of fission barriers in the mass region $150 < A < 210$. Using these data, a statistical model utilizing the barrier calculations of Sierk has been developed, and the sensitivity of the calculations to various input assumptions has been tested. The results yielded good qualitative agreement between data and calculations for a wide variety of heavy-ion-induced fission reactions leading to composite systems of mass 158, 186, 204, 206, 208, and 210. It was not necessary to introduce an arbitrary normalization factor for the fission barrier.

II. EXPERIMENTAL

The experimental setup is illustrated schematically in Fig. 1. Coincident fission fragments are detected in multiwire proportional counters (MWPC's) (Ref. 13) (STOP 1 and STOP 2) that yield two-dimensional position signals and a fast signal. The time-of-flight (TOF) for each fragment is determined using a start signal generated by a thin ($\sim 200 \mu\text{g}/\text{cm}^2$) MWPC (Ref. 14) that is placed

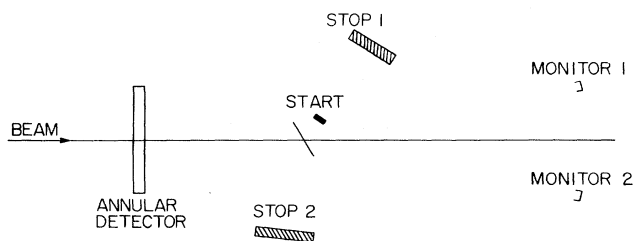


FIG. 1. Schematic diagram of the experimental setup.

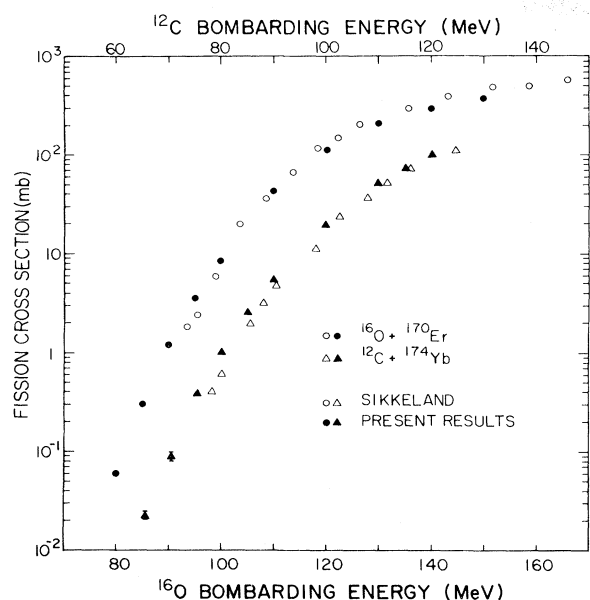


FIG. 2. Fission cross sections from the present experiment compared to previous measurements of Sikkeland *et al.* (Ref. 2).

close to the target. Approximate flight paths were 21 cm for fragment 1 (START to STOP 1) and 17 cm for fragment 2 (target to STOP 2). The overall resolution of the TOF measurements was ~ 400 psec, which was sufficient to ensure that measured widths of total kinetic energy, mass, and momentum transfer distribution were limited by the dispersion from the neutrons emitted from the fragments. The MWPC's had active areas of 2×2 cm² and 10×8 cm² for START and STOP, respectively. This

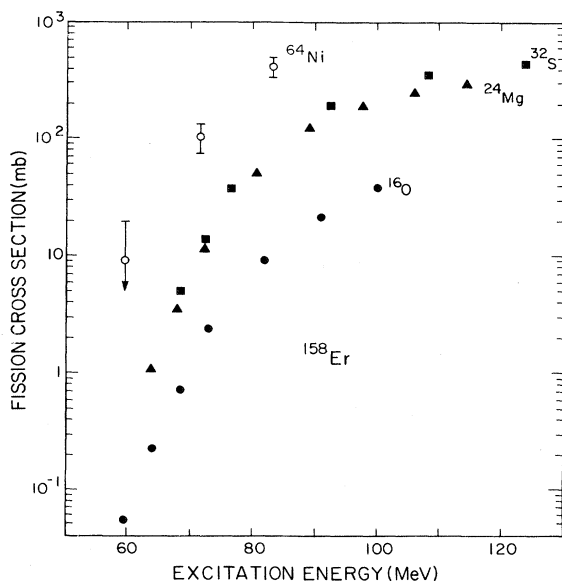


FIG. 3. Fission cross sections as a function of compound nucleus excitation energy for reactions leading to the composite system ^{158}Er from bombardments with projectiles from ^{16}O through ^{64}Ni .

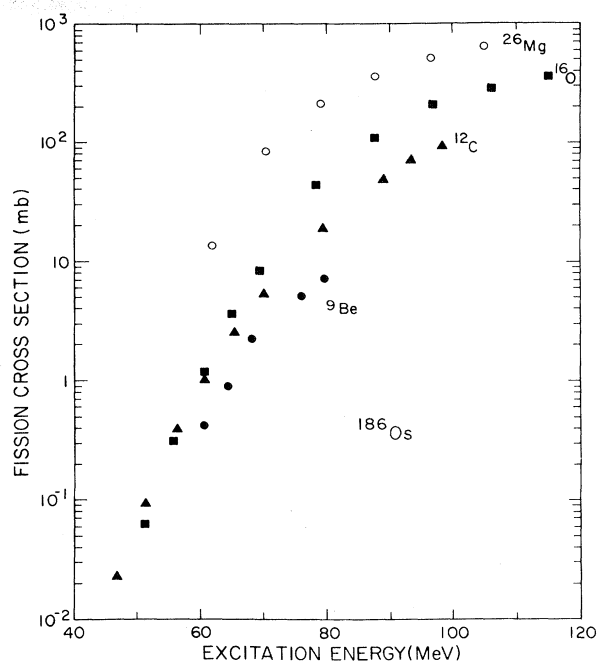


FIG. 4. Fission cross sections as a function of compound nucleus excitation energy for reactions leading to the composite system ^{186}Os from bombardments with projectiles from ^9Be through ^{26}Mg .

resulted in an angular acceptance $\Delta\theta$, $\Delta\phi$ of 22° , 18° (fragment 1) and 33° , 26° (fragment 2). Detector 1 was placed at a mean angle of 57° , and the angle of detector 2 was determined from the kinematics of the various reactions.

The electronic logic was set up so that events were recorded on magnetic tape whenever either STOP 1 or STOP 2 registered a pulse. Then, position and analog sig-

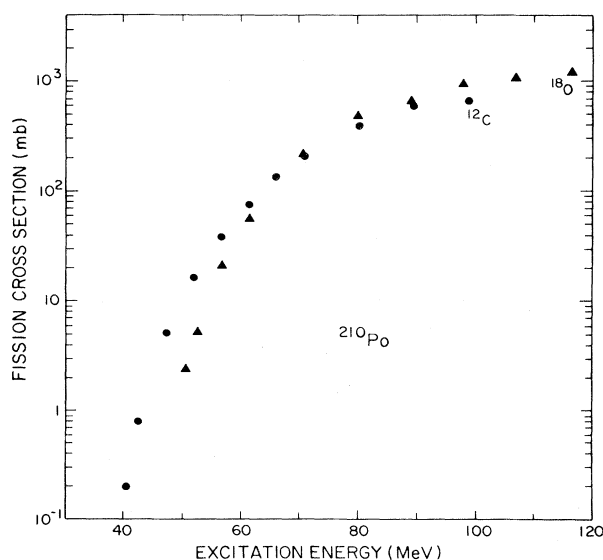


FIG. 5. Fission cross sections as a function of compound nucleus excitation energy for reactions leading to the composite system ^{210}Po from bombardments with ^{12}C and ^{18}O .

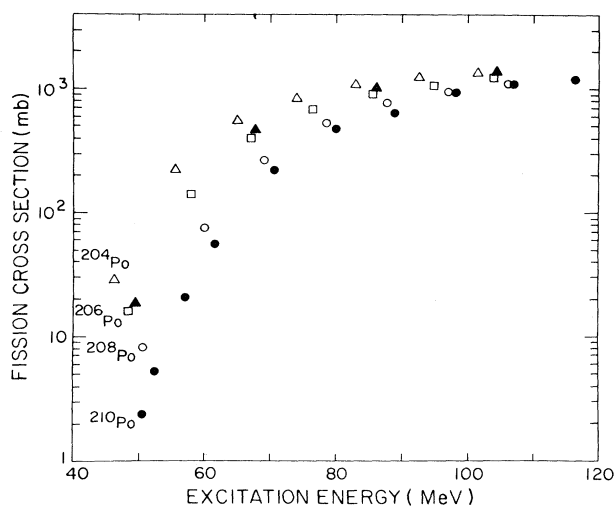


FIG. 6. Fission cross sections as a function of compound nucleus excitation energy for reactions leading to various Po isotopes. Closed symbols refer to ^{18}O bombardments and open symbols to ^{16}O bombardments. Note that ^{206}Po data was obtained with both ^{16}O and ^{18}O bombardments.

nals were recorded on magnetic tape from all detectors. In all detectors fission fragment pulse heights were well above noise, and fragments could be easily recorded with 100% efficiency. Spectra from monitor detectors at $\pm 12^\circ$ were also recorded on magnetic tape with the same dead time as the fission measurements.

The positions in the STOP detectors were calibrated using a precisely positioned mask with a pattern of 1.5-mm-diam holes. The TOF spectra were calibrated with a ^{252}Cf source and a time-to-amplitude converter (TAC) calibrator.

In the analysis of the cross-section data, the events were first replayed from magnetic tape with a gate on single events detected in a small, well-defined area of detector 1, and a check was made that the complementary fragments associated with these events struck an active area of detector 2 with greater than 95% probability. Then the various possible correlations between fragment 1 and fragment 2 were checked and sometimes subjected to gates so that any noise or, in some cases, fission from small target contaminants could be easily eliminated. The correlations used for this purpose were X_1 vs X_2 , Y_1 vs Y_2 , TOF_1 vs TOF_2 , and θ_1 vs θ_2 (or the calculated momentum-transfer distribution).

Absolute differential cross sections were calculated using measured geometries and assuming Rutherford scattering in the monitor detectors. Total fission cross sections were calculated assuming an angular distribution proportional to $1/\sin\theta$. This procedure seemed most reasonable because detailed angular distribution data are not available at this time and the assumption of a $1/\sin\theta$ dependence will make any future corrections based on new experimental data particularly simple. From systematic measurements relative to a current integrator and various repeat measurements, we estimate that the systematic un-

certainty in relative measurements for a particular projectile-target combination is less than 5%. The absolute uncertainty in the measured cross sections is believed to have a systematic uncertainty of less than 10% (except that in all cases the $1/\sin\theta$ angular distribution is assumed). In the data presentations statistical uncertainties greater than 5% are indicated.

The targets used in these experiments were generally in the 100 to 250 $\mu\text{g}/\text{cm}^2$ thickness range. In some cases the targets were in the form of oxides on carbon backings, but the presence of light elements did not affect the absolute fission cross-section determinations.

III. RESULTS

The cross sections obtained in these experiments are shown in Figs. 2–6 and are tabulated in Table I. The ^{16}O and ^{12}C reactions leading to ^{186}Os overlap previous experiments of Sikkeland *et al.*,^{2,3} and Fig. 2 shows a comparison to their measurements. At the higher energies, the present measurements are 10–20% lower for the ^{16}O bombardments and 5–10% higher for the ^{12}C measurements. At the lowest energies, the present measurements are consistently higher, but this could easily arise from the uncertainties and spread in the bombarding energies for the Sikkeland measurements, since they were forced to vary the energy using absorber foils. There were also possible uncertainties in the primary energies available from the heavy-ion linear accelerator (HILAC) at that time. At the lowest energies, the Sikkeland data were converted to cross sections assuming σ_f was up to 15% lower than the value obtained with a $1/\sin\theta$ angular distribution; this could also contribute to the deviations shown in Fig. 2. However, it should be stressed that the overall agreement between these two measurements is remarkably good. This point is especially important because, with the exception of the present data, the experiments of Sikkeland *et al.*^{2,3} form the broadest available data set on heavy-ion-induced fission in rare earth nuclei.

The fission cross sections for composite systems ^{158}Er and ^{186}Os are shown in Figs. 3 and 4 as a function of the excitation energy of the compound nucleus. In these cases the angular momentum dependence of the fission cross section is illustrated dramatically by the increase in cross section with increasing projectile mass at a fixed excitation energy. It is seen that the data show a consistent pattern.

Figures 5 and 6 show the results for C and O reactions leading to various Po systems. For ^{210}Po , the ^{18}O cross section is cut off by the Coulomb barrier, so the angular momentum effects are not so obvious. The increase in cross section with decreasing composite mass shown in Fig. 6 is an effect of both moving away from the double closed shell (^{208}Pb) and the increasing fissility (Z^2/A).

In the interpretation of the cross sections it becomes important to try to identify any components that might arise from fission following incomplete fusion. Figure 7 shows distributions of the velocity of the fissioning system relative to the compound nucleus velocity for the highest energy C and O reactions leading to the most fissionable system (^{210}Po) and for $^{16}\text{O} + ^{232}\text{Th}$. In the ^{232}Th case, there

TABLE I. Experimental cross sections. Statistical errors are less than 5% except where indicated. Absolute fission cross sections are estimated from $d\sigma/d\Omega$ at 57° laboratory angle using an assumed angular distribution proportional to $1/\sin\theta$. Bass cross sections (Ref. 18) used for the statistical model calculations are also included.

E_L (MeV)	E^* (MeV)	σ_f (mb)	σ_{Bass} (mb)	E_L (MeV)	E^* (MeV)	σ_f (mb)	σ_{Bass} (mb)
$^{16}\text{O} + ^{142}\text{Nd}$							
95	59.6	0.055±0.007	990	110	78.6	43.2	1208
100	64.1	0.230±0.020	1090	120	87.8	113.	1366
105	68.6	0.740±0.050	1190	130	96.9	209.	1438
110	73.1	2.37	1265	140	106.1	294.	1500
120	82.1	9.2	1350	150	115.2	371.	1562
130	91.1	21.6	1412				
140	100.1	38.5	1462				
$^{24}\text{Mg} + ^{134}\text{Ba}$							
120	63.8	1.13 ±0.30	684	120	62.0	13.6 ±1.5	492
125	68.0	3.57 ±0.40	792	130	70.6	84.	745
130	72.3	11.4	890	140	79.2	208.	958
140	80.7	51.6	1050	150	87.8	363.	1123
150	89.2	124.	1190	160	96.4	515.	1249
160	97.7	188.	1265	170	105.0	651.	1374
170	106.2	251.	1330				
180	114.7	302.	1375				
$^{32}\text{S} + ^{126}\text{Te}$							
150	68.5	5.0	506				
155	72.4	13.7	685				
160	76.4	38.6	773				
180	92.4	195. ±20	1060				
200	108.3	372. ±40	1212				
220	124.3	445. ±50	1370				
$^{64}\text{Ni} + ^{94}\text{Zr}$							
250	59.3	9 ⁺¹¹ ₋₉	471				
270	71.2	105 ±30	721				
290	83.1	420 ±80	921				
$^9\text{Be} + ^{177}\text{Hf}$							
64	60.7	0.42 ±0.07	1371				
68	64.5	0.90 ±0.11	1471				
72	68.3	2.20 ±0.16	1548				
80	75.9	5.10	1640				
84	79.7	7.2	1670				
$^{12}\text{C} + ^{174}\text{Yb}$							
65	46.8	0.023±0.003					
70	51.5	0.092±0.010					
75	56.2	0.390	922				
80	60.8	0.99	1071				
85	65.5	2.50	1195				
90	70.2	5.38	1298				
100	79.6	19.4	1463				
110	88.9	49.1	1518				
115	93.6	71.5	1545				
120	98.3	95.1	1572				
$^{16}\text{O} + ^{170}\text{Er}$							
80	51	0.06 ±0.01					
85	55.8	0.31 ±0.02	559				
90	60.4	1.19	722				
95	64.9	3.64	861				
100	69.5	8.5	999				
$^{12}\text{C} + ^{198}\text{Pt}$							
				55	37.9	0.003±0.002	
				58	40.7	0.20 ±0.02	
				60	42.6	0.79 ±0.08	10
				65	47.3	5.1	304
				70	52.0	16.6	549
				75	56.7	38.7	755
				80	61.4	74.7	930
				85	66.1	136.	
				90	70.9	209.	1207
				100	80.3	399.	1408
				110	89.7	601.	1495
				120	99.1	775.	1587
$^{18}\text{O} + ^{192}\text{Os}$							
				78	50.6	2.4	
				80	52.4	5.3	108
				85	57.0	21.0	
				90	61.6	57.	542
				100	70.7	221.	874
				110	79.9	486.	1133
				120	89.0	753.	1300
				130	98.2	963.	1494
				140	107.3	1100.	1570
				150	116.4	1230.	1649
				E_L (MeV)	E^* (MeV)		σ_f (mb)
				$^{16}\text{O} + ^{192}\text{Os}$			
				80	50.7		8.3
				90	60.0		76.2
				100	69.2		270.
				110	78.4		540.
				120	87.7		770.
				130	96.9		944.
				140	106.1		1130.

TABLE I. (Continued.)

E_L (MeV)	E^* (MeV)	σ_f (mb)
$^{16}\text{O} + ^{190}\text{Os}$		
80	48.7	16.4
90	57.9	139.
100	67.1	405.
110	76.4	701.
120	85.6	914.
130	94.8	1070.
140	104.0	1260.
$^{18}\text{O} + ^{188}\text{Os}$		
80	49.4	18.9
100	67.7	486.
120	85.9	1035.
140	104.2	1310.
$^{16}\text{O} + ^{188}\text{Os}$		
80	46.3	28.9
90	55.6	230.
100	64.8	545.
110	74.0	855.
120	83.2	1070.
130	92.4	1260.
140	101.6	1380.

is clearly a small component ($\sim 10\%$) that is consistent with incomplete fusion involving a forward-going alpha particle. The ^{232}Th results came from analysis of data from a ^{232}Th contaminant in one Nd target. There is no evidence that such reactions lead to fission in ^{210}Po . How-

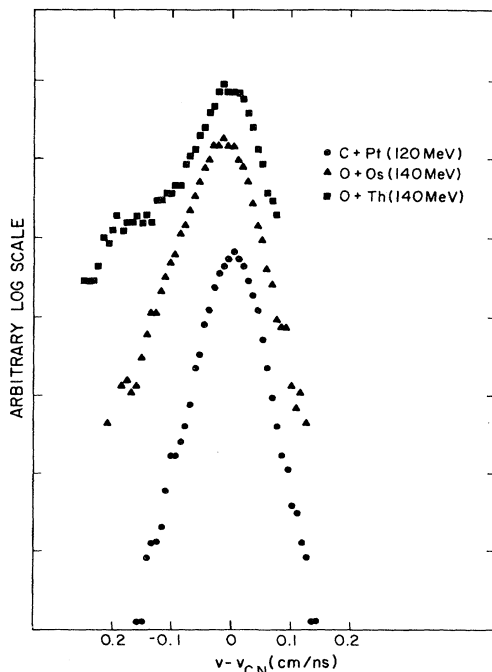


FIG. 7. Distribution of velocities for the fissioning system for the indicated reactions. Values are relative to the compound nucleus velocity v_{CN} resulting from full momentum transfer.

ever, the $^{18}\text{O} + ^{192}\text{Os}$ data do show a slight skewing toward lower velocities that would be qualitatively consistent with preequilibrium nucleon emission of the magnitude reported previously.^{15,16}

IV. THEORETICAL COMPARISONS

A. General considerations

The major objective of this experiment was to provide a comprehensive data base of fission cross sections against which various theoretical models and concepts could be tested. In this context a statistical model code has been developed incorporating our current best estimates of the important physical parameters. This code uses Monte Carlo techniques and has been described previously in general technical terms.¹⁷ For the following, we will discuss mainly those aspects relevant to the current calculations of fission cross sections. These calculations necessarily involve both details of the compound nucleus formation process and the relative competition between fission and other modes in the compound nucleus decay process. Since the fission barrier is a strong function of angular momentum, it is particularly necessary to incorporate angular momentum effects as realistically as possible. By considering deviations between the predictions and the experimental data, we would hope to identify weaknesses in the theoretical formulation and possibly point out new experimental approaches which might provide more stringent tests of our current theoretical concepts. In the following sections, we will discuss the physical concepts that go into the development of the statistical model, show a comparison of predictions with experimental data, and discuss the significance of the comparisons.

B. Theoretical model

1. Formation of compound nucleus—fusion

Any model of fusion-fission must begin by estimating the fusion cross section as a function of angular momentum. We have chosen for fusion cross section estimates the most recent model proposed by Bass,¹⁸ which gives a description of the fusion cross sections in this mass and energy region to an accuracy of the order $\pm 10\%$.

Near threshold, the calculated fission cross sections are very sensitive to that tail of the angular momentum distribution for the fused system. This is because of the rapid change in the fission probability in the angular momentum region where the fission barrier crosses the neutron binding energy. In the calculations the fusion cross section was parametrized as

$$\sigma_{\text{fus}} = \pi \lambda^2 \sum_{l=0}^{\infty} (2l+1) T(l),$$

where

$$T(l) = \frac{1}{1 + \exp(l - l_{cr})/\delta l}.$$

The quantity δl was treated as an adjustable parameter, and its significance and range of values are discussed below. The fusion cross section, obtained from the Bass model, was used to determine l_{cr} .

An implicit assumption in our parametrization is that the entire fusion cross section as obtained from the Bass model¹⁸ corresponds to complete fusion. However, the Bass model is a parametrization which has been adjusted to fit experimental fusion cross section measurements that may contain both complete and incomplete fusion components. For C and O projectiles, the thorium data in Fig. 7 suggest that incomplete fusion components could be of the order of 10%. For heavier projectiles, incomplete fusion effects are unknown, but because of the generally lower energy per nucleon relative to the Coulomb barrier, we would expect them to be less significant.

At the highest energies for S and Ni projectiles, the angular momenta become high enough so that "extra push" effects^{19,20} could cause a decrease in the fusion cross section below the Bass model predictions. For our highest energy Ni reaction, the model of Swiatecki²⁰ would predict a 15–20% lowering of the fission cross section.

Because the magnitudes of the incomplete fusion and "extra push" effects^{19,20} are expected to be similar to the systematic uncertainties in the Bass model, and because these effects are both poorly understood in a quantitative sense, we have chosen to neglect them in the formulation of our current version of a theoretical statistical model.

2. Decay of the compound nucleus—fission

In order to calculate the total fission cross section, it is necessary to estimate the branching ratios for fission relative to particle emission as a function of angular momentum and excitation energy. The basic inputs for such a calculation are the ground state masses of the relevant nuclei, the fission barriers as a function of mass and angular momentum, and the level densities at both the ground state and saddle-point deformations. From this input, a Monte Carlo method is then used to estimate the contribution from fission summed over the particle deexcitation cascade.

The fission barriers are taken from the calculations of Sierk¹² for the systems ¹⁵⁸Er, ¹⁸⁶Os, and ²¹⁰Po. These barriers are obtained from a model of rotating nuclei which incorporates effects due to the finite range of the nuclear force and the diffuseness of the nuclear surface on the Coulomb, surface, and rotational energies. Effects due to possible axially asymmetric deformations are also taken into account. When compared to previous calculations (CPS),¹¹ the results show a reduction in the fission barrier heights of the order of 15% for zero angular momentum and relatively larger effects at the high angular momenta which become important in these heavy ion reactions. Calculations based on a similar model but with a different shape parametrization have also been reported by Mustafa *et al.*²¹ The Sierk barriers have been shown⁹ to give a good representation of ¹²C and ²⁰Ne induced fission excitation functions leading to the composite system ¹⁵³Tb and ¹⁸¹Re.

For the dependence of the nuclear state density on exci-

tation energy, $\omega(E)$, two extreme prescriptions were used. The first was a simple Fermi gas estimate which should be appropriate at high temperatures where shell and pairing effects have washed out. In this case, excitation energies were measured from the appropriate liquid drop mass surface. This meant that the effective ground state used for level densities for particle emission was shifted from the true ground states by the shell plus pairing energy. This formulation would be expected to be most appropriate at high excitation energies. In this formulation, the ratio of level density parameters a_f/a_n is adjustable over a narrow region but would be expected to be close to 1.00.

In the second prescription, $\omega(E)$ was generated from single-particle level schemes, similar to the approach employed in the analysis of actinide fission probabilities.¹ However, the uncertainties in this approach are much larger than in the previous application to actinide data because: (1) Detailed mappings of the relevant shell corrected potential energy surfaces are not available; (2) it is necessary to consider much higher excitation energies than in the actinide case so that the approximate cancellation of shell and pairing effects is no longer relevant; and (3) there is little experimental or theoretical guidance on how to handle collective enhancement effects and how these enhancements wash out at higher energies. Therefore, the single-particle-based level densities described below should be considered primarily as simply an alternative formulation of the level density function to give an indication of the sensitivity of calculations to the level density function.

For the light particle decay channels, the level densities were obtained using single particle spectra from Nix²² for Po and Os systems and from a Nilsson model calculation²³ for Er. The code of Moretto²⁴ was then used to generate total nuclear state densities $\omega(E)$. In all cases, we used single particle spectra at zero deformation (i.e., spherical shape) to generate the microscopic level densities. In the Po case, the proximity of the doubly magic ²⁰⁸Pb shell had a large influence on the state densities. In this case, state densities were calculated for each isotope in the decay chain. For Os and Er systems the same state densities were used for all isotopes.

For the fission decay channels, microscopic level densities at the saddle point are required. For the Er and Os systems we found that $\omega(E)$ had only a small dependence on deformation and $\omega(E)$ was taken as the same function used for the ground state deformation. For Po, the deformation dependence of $\omega(E)$ was studied and a function appropriate to the saddle point deformation was used. In all cases, the excitation energies at the fission barrier were measured from the liquid drop saddle point because the shell correction at this deformation is expected to be small and could not be estimated reliably enough to exclude a zero value.

In keeping with the qualitative nature of these level density estimates, it was assumed that there was no large angular momentum dependence to the shell correction so that the angular momentum dependent level density $\rho(E, J)$ was approximated by

$$\rho(E, J) = \frac{2J+1}{\sqrt{8\pi\sigma^3}} \omega[E - E_{rot}(J)].$$

In these calculations, the nuclear state density $\omega(E)$ was taken either from the microscopic formulation described above or from a Fermi gas model. The rotational energy $E_{\text{rot}}(J)$ was taken from CPS calculations¹¹ at both the ground state and saddle point deformations.

This level density calculation is equivalent to the spherical case described in previous publications,^{26,27} except for the inclusion of a macroscopic rotational energy instead of a microscopically calculated spin cutoff factor. Our level density formulation does not specifically include any collective enhancement effects of the type that were found essential to a quantitative interpretation²⁷ of low excitation, low angular momentum actinide data. In fact, if collective enhancements were included at only the saddle point deformation, the generally good agreement between calculations and experiments that is shown below would be lost. Two possibilities exist: (1) The collective enhancement effects have been washed out at the relatively high excitation energies and angular momenta of primary concern here; and (2) the ground state and saddle point shapes for the high angular momenta in these reactions are both deformed so that the ratio of enhancement effects at the ground state and saddle point will be close to unity.

C. Comparisons to experimental data

We wish to emphasize that the purpose of the present model calculations was primarily to attempt a qualitative comparison to the experimental data and to test the sensitivity of the calculations to different models of the level densities. Further progress in the development of our model is limited by the fact that we do not have quantitative estimates for all of the relevant shell energies or a complete understanding of the effect of shells and collective enhancements on level densities at moderate to high excitation energies. These fundamental questions and similar uncertainties in our understanding of the fusion process and the fission barrier functions should be considered when comparing the calculations to the experimental results presented here.

Figures 8–11 show comparisons of the data from this experiment with fission cross sections calculated as described above. Also shown are comparisons to ^4He induced fission²⁵ for ^{186}Os and ^{210}Po , ^{11}B induced fission³ for ^{186}Os , and recent ^{19}F and ^{30}Si reactions¹⁰ leading to ^{200}Pb . The data of Hinde *et al.*¹⁰ for ^{200}Pb were especially valuable since they also measured evaporation residue cross sections, which allowed a more comprehensive test of the model calculations. In this case, the calculated evaporation residue cross sections agreed with their data to better than 10%. It should be noted that the Bass fusion cross sections¹⁸ used in this model are qualitatively different from an earlier formulation²⁸ that was used for comparison in the paper of Hinde *et al.*¹⁰ The parameters used in the model calculations are listed in Table II. It should be noted that a_f/a_n is always near 1.0; ΔE is determined from mass tables and is not adjustable. In the case of the microscopic based level densities, there is no adjustable parameter equivalent to a_f/a_n . In the threshold region, the angular momentum dispersion in the fusion

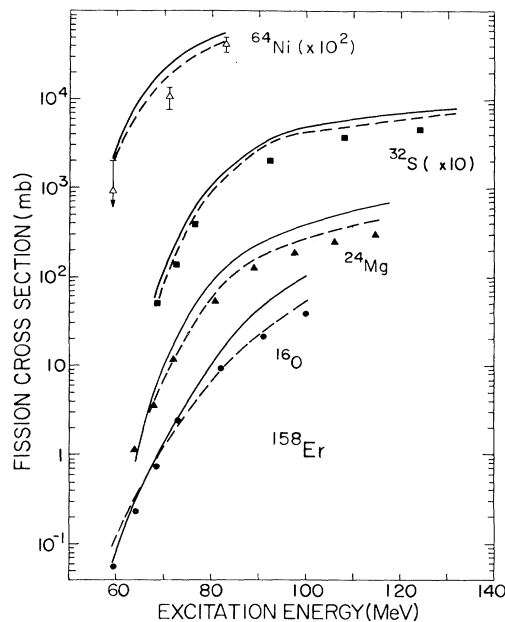


FIG. 8. Calculated fission cross sections compared to experimental data for the composite system ^{158}Er . Solid lines use Fermi gas level densities and dashed lines use microscopic level densities (see text).

cross sections becomes important. The δI values shown in Table II were obtained by adjusting δI to obtain the best fits to the low energy portions of the excitation functions. The large values of δI for Mg, S, and ^{18}O could be indicative of dynamic and/or static deformations affecting the threshold region in a manner similar to that observed previously⁶ for $^{32}\text{S} + ^{144,154}\text{Sm}$ reactions where changes in target deformations were shown to be imported. The sen-

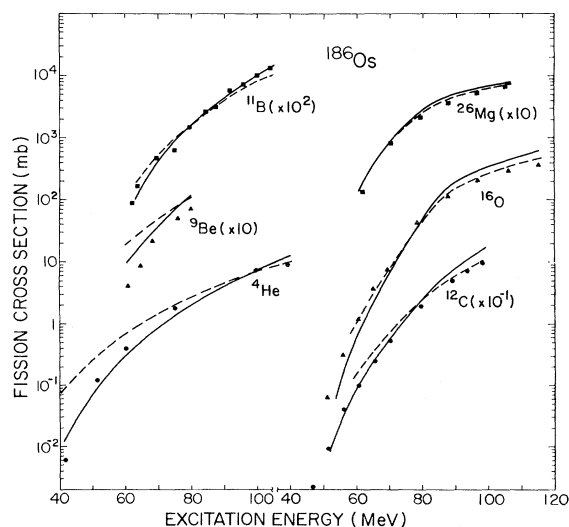


FIG. 9. Calculated fission cross sections compared to experimental data for the composite system ^{186}Os . Solid lines use Fermi gas level densities and dashed lines use microscopic level densities (see text). Data for ^4He and ^{11}B reactions were taken from Refs. 25 and 3, respectively.

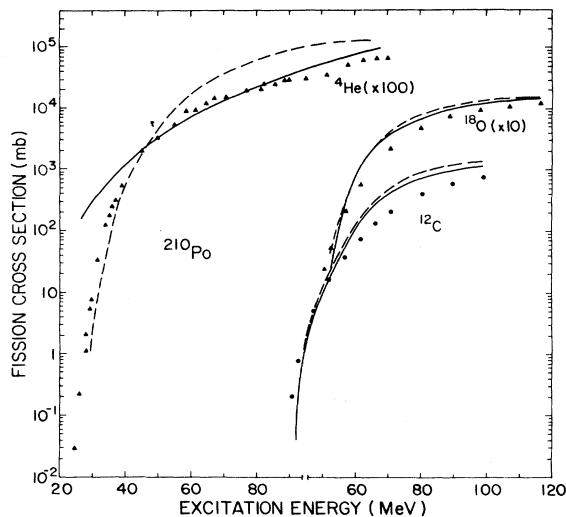


FIG. 10. Calculated fission cross sections compared to experimental data for the composite system ^{210}Po . Solid lines use Fermi gas level densities and dashed lines use microscopic level densities (see text). Data for ^4He reaction were taken from Ref. 25.

sitivity of the calculated cross sections to δl is shown for two cases in Fig. 12.

The calculated cross sections shown in Figs. 8–11 agree remarkably well with experimental data over a very broad region. The significance of this agreement is further illustrated in Fig. 13, which shows calculations with barriers from Sierk,¹² Mustafa *et al.*,²¹ and Cohen, Plasil, and Swiatecki.¹¹ In these calculations the microscopic-based level densities were used. The angular momentum dependence of the barrier functions is shown in Fig. 14. The success in describing data ranging from the rare earth re-

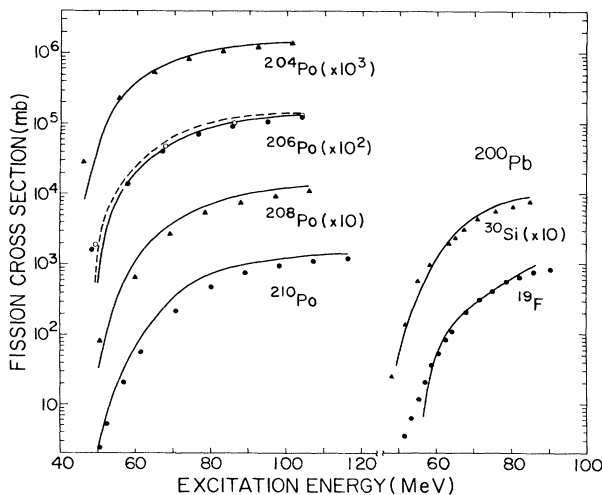


FIG. 11. Calculated fission cross sections compared to experimental data for Po isotopes and ^{200}Pb (Ref. 10). Calculations use Fermi gas level densities. For ^{206}Po , the solid curve and solid points are for the reaction with ^{16}O projectiles while the dashed curve and open points are for ^{18}O projectiles.

TABLE II. Parameters in statistical model calculations.

Composite system	Projectile	a_f/a_n^a	ΔE^b (MeV)	δl^c (\hbar)
^{158}Er	^{16}O	1.000	1.4	0.5
	^{24}Mg			3.1
	^{32}S			3.2
	^{64}Ni			0.5
^{186}Os	^4He	1.015	1.5	1.5
	^9Be			1.5
	^{11}B			0.5
	^{12}C			1.5
	^{16}O			1.5
	^{26}Mg			6.0
^{210}Po	^4He	1.000	10.0	0.5
	^{12}C			0.5
	^{18}O			3.5

^aIn all cases $a_n = A/7.5$.

^b ΔE is the energy difference between the liquid drop ground state mass and the true ground state mass.

^c δl is the dispersion factor in the critical angular momentum as described in the text.

gion to the closed shell Pb-Po region and for bombarding particles ranging from ^4He to ^{64}Ni indicates that the overall excitation energy, angular momentum, and fissility dependences of this model utilizing the Sierk barriers¹² must be reasonably correct. Nevertheless, there are some systematic deviations that will be discussed below as indications for possible fruitful future extensions to both theoretical and experimental programs in this area.

In the case of the ^4He and ^9Be induced reactions at the lower energies, the angular momenta brought in are well below the regions where the fission barrier has decreased to the order of the neutron binding energies. Thus, the

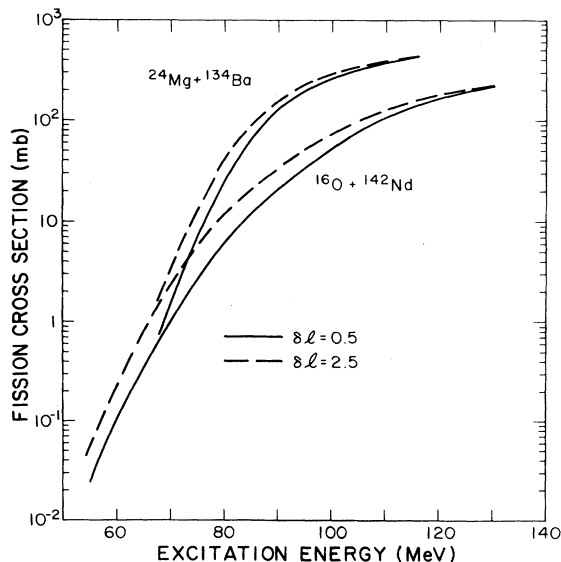


FIG. 12. Sensitivity of the theoretical calculations to value of δl for two reactions leading to ^{158}Er .

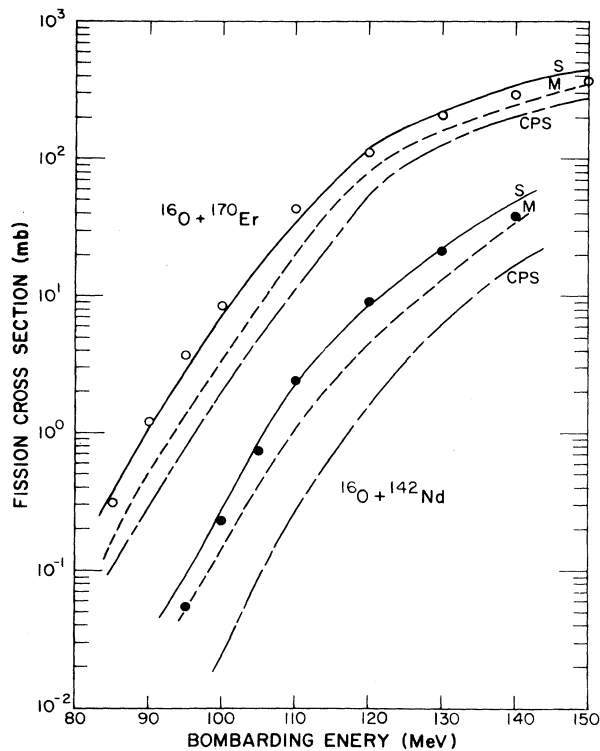


FIG. 13. Comparison of experimental data from two reactions with predictions from the theoretical statistical model with angular momentum dependent fission barriers from Sierk (S) (Ref. 12); Mustafa *et al.* (M) (Ref. 21), and Cohen, Plasil, and Swiatecki (CPS) (Ref. 11). Calculations use microscopic level densities.

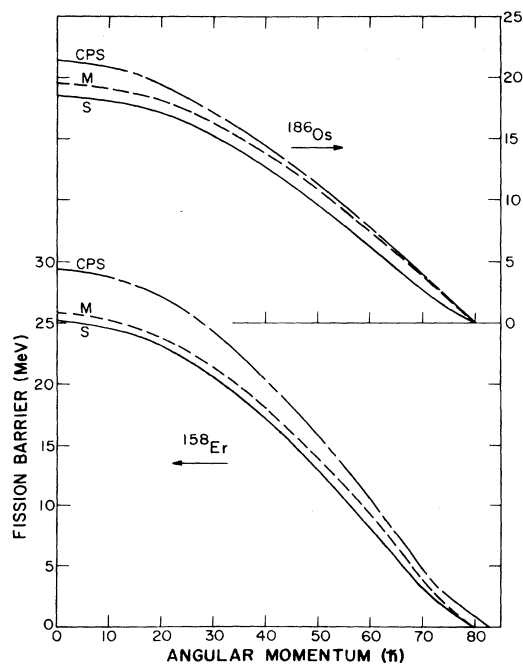


FIG. 14. Calculated fission barriers as a function of angular momentum from Sierk (S) (Ref. 12), Mustafa *et al.* (M) (Ref. 21), and Cohen, Plasil, and Swiatecki (CPS) (Ref. 11).

fission cross section tends to be a sum over l values for which each term has a small fission probability. In this case, the data in principle could test the fission barrier calculations at low angular momentum, but the calculations are also sensitive to the high energy behavior of the level densities, which may not be quantitatively understood. In the ^{210}Po and ^{186}Os cases, it is seen that there are substantial deviations between calculations with the two extreme level density formulations. An additional uncertainty in the ^4He and ^9Be cases is the applicability of the Bass model¹⁸ in estimating the fusion cross section. In fact, the systematic overprediction of σ_f for the ^9Be reaction (Fig. 9) could be due to an overprediction of the fusion cross section. Recent data²⁹ for the $^9\text{Be} + ^{40}\text{Ca}$ reaction indicate an unusually small fusion cross section. Thus, it appears that more experimental (σ_{fus}) and theoretical insights are necessary before a further quantitative test of the low l portion of the fission barrier calculations is possible.

For the higher energies and heavier projectiles a very different situation exists. Here, the angular momentum distribution extends into the region of high fission probabilities. In these cases, the fission cross sections are dominated by a sum of $\sigma(l)$ for angular momenta greater than

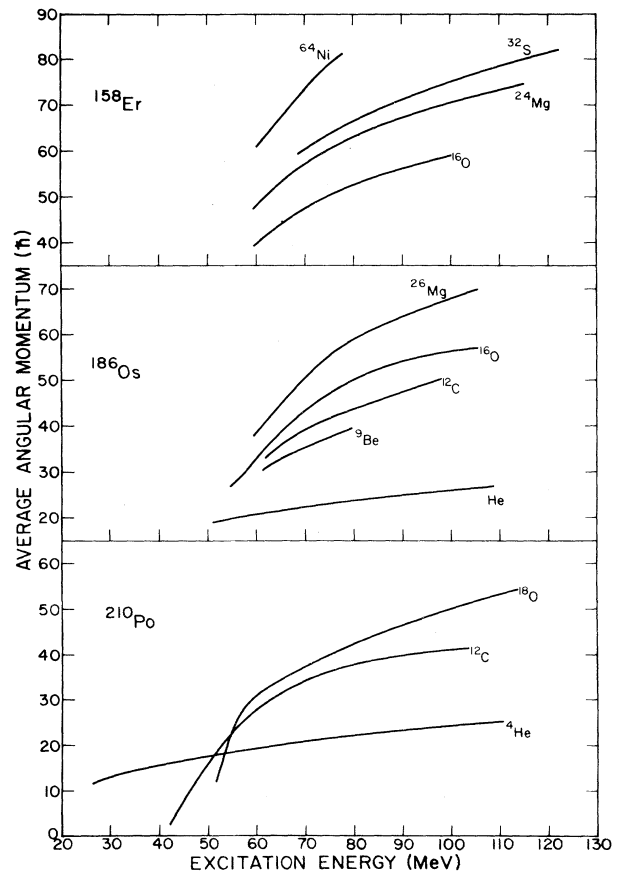


FIG. 15. The average angular momentum leading to fission from the statistical model calculations shown in Figs. 8–10 using the Fermi gas based level density functions.

the value for which $B_f = B_n$. If $B_f(l)$ is rapidly changing in this region, then the level density functions are of less importance. In these cases, the theoretical calculation is most sensitive to the calculated B_f in the angular momentum region where B_f crosses B_n and to the calculated fusion cross section. The differences in angular momenta involved in different reactions leading to the same composite systems are illustrated in Fig. 15. Figure 15 shows the average angular momentum leading to fission from the statistical model calculations.

The case of the reaction $^{64}\text{Ni} + ^{94}\text{Zr} \rightarrow ^{158}\text{Er}$ is qualitatively different from the other cases involving lighter projectiles. Here, the reaction is dominated by quasi-elastic and deeply inelastic reactions, but it was possible to isolate a symmetric fissionlike component, which is shown in Fig. 8. The increased uncertainty in isolating the symmetric fission component is reflected by the relatively larger error bars shown in Fig. 8.

V. SUMMARY

In this paper we have presented a comprehensive set of data on fission cross sections for Po, Os, and Er isotopes excited in a variety of heavy-ion reactions induced by projectiles from ^9Be through ^{64}Ni . The experimental results clearly show the qualitative effects of angular momentum, excitation energy, and fissility on the fission cross section. They provide an ideal testing ground for theoretical models of fission in this mass region.

The results are compared to predictions of a theoretical model incorporating a new calculation of angular-momentum-dependent fission barriers by Sierk.¹² The predictions show remarkable agreement with experimental results without the need for arbitrary normalization factors for the calculated fission barrier function. For the reactions induced by carbon and heavier projectiles, the fission cross section is primarily sensitive to angular momen-

ta near and above the value where the fission barrier equals the neutron binding energy. These data do not effectively test the barrier calculations for lower angular momenta. Previous data on fission induced by ^4He particles²⁵ do test the lower angular momentum region and show a qualitative agreement between predictions and data. However, uncertainties in the relevant level density functions and fusion cross sections limit the ability to test the barrier function in this case.

Within the accuracy of the comparisons, there is no need to invoke shell corrections at the saddle point. More quantitative tests of the calculated barriers would require experimental data on the evaporation residue cross sections, a knowledge of the properties of any incomplete fusion effects, and an improved model for the level densities used in estimating $\Gamma_f/\Gamma_{\text{tot}}$.

ACKNOWLEDGMENTS

This work was supported by the U.S. Department of Energy. We are particularly grateful to Ole Hansen, Craig Thorn, Harvey Wegner, and Roger Lee for their support and help during these measurements. It is a pleasure to acknowledge the many helpful, professional, and pleasant interactions with the Brookhaven National Laboratory (BNL) tandem operating staff. We benefited considerably from discussions with J. R. Nix and A. Sierk, and we are especially grateful for permission to use their calculated barrier functions before publication. We would also like to thank M. G. Mustafa for supplying fission barrier calculations for our systems. We are grateful to Judith Gursky for the production of most of the targets used in these measurements. One of the authors (Z.F.) wishes to thank the Physics Division of the Los Alamos National Laboratory for the hospitality extended to him during the course of this work.

*Present address: National Superconducting Cyclotron Laboratory, Michigan State University, East Lansing, MI 48823.

†Permanent address: Weizmann Institute of Science, Rehovot, Israel.

¹See, H. C. Britt, *Physics and Chemistry of Fission 1979* (IAEA, Vienna, 1980), Vol. I, p. 3; S. Bjørnholm and J. E. Lynn, *Rev. Mod. Phys.* **52**, 735 (1980), and references therein.

²T. Sikkeland, *Phys. Rev.* **135**, B669 (1964).

³T. Sikkeland, J. E. Clarkson, N. H. Steiger-Shafir, and V. E. Viola, *Phys. Rev. C* **3**, 329 (1971).

⁴M. Beckerman and M. Blann, *Phys. Rev. C* **17**, 1615 (1978).

⁵F. Plasil, R. L. Ferguson, R. L. Hahn, F. E. Obenshain, F. Pleasonton, and G. R. Young, *Phys. Rev. Lett.* **45**, 333 (1980).

⁶B. B. Back, R. R. Betts, W. Henning, K. L. Wolf, A. C. Mignerey, and J. M. Lebowitz, *Phys. Rev. Lett.* **45**, 1230 (1980).

⁷S. E. Vigdor and H. J. Karwowski, *Phys. Rev. C* **26**, 1068 (1982); **26**, 1035 (1982).

⁸M. Blann and T. T. Komoto, *Phys. Rev. C* **26**, 472 (1982).

⁹F. Plasil, J. R. Beene, B. Cheynis, R. L. Ferguson, F. E. Obenshain, A. J. Sierk, G. R. Young, A. Gavron, and G. A. Petitt, *Proceedings of the Workshop on Nuclear Dynamics*,

1982, Lawrence Berkeley Laboratory Report LBL 14138, 1982, p. 61.

¹⁰D. J. Hinde, J. R. Leigh, J. O. Newton, W. Galster, and S. Sie, *Nucl. Phys.* **A385**, 109 (1982); D. J. Hinde, J. O. Newton, J. R. Leigh, and R. J. Charity, **A398**, 308 (1983).

¹¹S. Cohen, F. Plasil, and W. J. Swiatecki, *Ann. Phys. (N.Y.)* **82**, 557 (1974).

¹²A. Sierk, private communication.

¹³J. van der Plicht and A. Gavron, *Nucl. Instrum. Methods* (to be published).

¹⁴A. Breskin, R. Chechik, and N. Zwing, *Nucl. Instrum. Methods* **165**, 125 (1979).

¹⁵A. Gavron, J. R. Beene, B. Cheynis, R. L. Ferguson, F. E. Obenshain, F. Plasil, G. R. Young, G. A. Petitt, M. Jääskeläinen, D. G. Sarantites, and C. F. Maguire, *Phys. Lett.* **47**, 1255 (1981).

¹⁶E. Duek, L. Kowalski, M. Rajagopalan, J. M. Alexander, D. Logan, M. S. Zisman, and M. Kaplan, *Z. Phys. A* **307**, 221 (1982).

¹⁷A. Gavron, *Phys. Rev. C* **21**, 230 (1980); Y. Eyal and M. Hillman, evaporation code JULIAN (unpublished).

¹⁸R. Bass, *Phys. Rev. Lett.* **38**, 265 (1977).

- ¹⁹J. R. Nix, *Annu. Rev. Nucl. Sci.* **22**, 65 (1972).
- ²⁰W. J. Swiatecki, *Nucl. Phys. A* **376**, 275 (1982).
- ²¹M. G. Mustafa, P. A. Baisden, and H. Chandra, *Phys. Rev. C* **25**, 2524 (1982), and private communication.
- ²²J. R. Nix, private communication.
- ²³S. G. Nilsson, C. F. Tsang, A. Sobieszewski, Z. Szymanski, S. Wycech, C. Gustafson, I. Lamm, P. Möller, and B. Nilsson, *Nucl. Phys. A* **13**, 1 (1969).
- ²⁴L. G. Moretto, private communication.
- ²⁵A. Khodai-Joopari, Ph.D. thesis, University of California Report UCRL-16489, 1966 (unpublished); L. G. Moretto, S. G. Thompson, J. Routti, and R. C. Gatti, *Phys. Lett.* **38B**, 471 (1972).
- ²⁶H. C. Britt, M. Bolsterli, J. R. Nix, and J. L. Norton, *Phys. Rev. C* **7**, 801 (1973).
- ²⁷A. Gavron, H. C. Britt, E. Konecny, J. Weber, and J. B. Wilhelmy, *Phys. Rev. C* **13**, 2374 (1976).
- ²⁸R. Bass, *Nucl. Phys. A* **261**, 45 (1974).
- ²⁹J. S. Eck, A. R. Omar, J. R. Leigh, and T. R. Ophel, *Phys. Rev. C* **27**, 1807 (1983).